RSC Advances

ROYAL SOCIETY OF CHEMISTRY

www.rsc.org/advances

Journal Name

ARTICLE

Self-assembled Flower-like $ZnCo_2O_4$ Hierarchical Superstructures for High Capacity Supercapacitors

Received 00th January 20xx,
Accepted 00th January 20xx

DOI: 10.1039/x0xx00000x

www.rsc.org/

Satyajit Ratha, and Chandra Sekhar Rout*

Abstract. Self-assembled $ZnCo_2O_4$ nanosheets were synthesised by one-step hydrothermal method and its electrochemical supercapacitor properties were investigated in 2M aqueous KOH solution. Interesting capacitive properties were observed with superb cyclic stability even at a current density of 20 A/g. Specific capacitance value of 1691 F/g was obtained at a current density of 3.75 A/g with an energy density of ~57.4 Wh/Kg. The experimental findings provide useful insights in the design of supercapacitors for potential high performance energy storage application in future.

1. Introduction

The huge oppressive condition in recent years due to the tremendous requirement of energy is further worsened by the rapid depletion of non-renewable energy sources such as fossil fuels. In addition, complicated environmental issues are fast arising out of their continuous consumption, which have motivated intense search for cleaner, renewable and eco-friendly energy storage and conversion options. Solar cells,[1] fuel cells,[2] Li-ion batteries[3] and supercapacitors[4] are some of the promising alternatives that have gone under critical research in recent years. Owing to their intriguing and tunable physical and chemical properties, two dimensional materials (in various forms) have drawn copious amount of attention from the scientific community. These two dimensional materials have thus found some direct applications in such areas.[5,6] Among such two dimensional materials, graphene has been the most phenomenal since its discovery owing to its fascinating physical and chemical properties,[7–9] and has provided an ideal platform for the study of analogous two dimensional materials such as transition metal chalcogenides,[10]metal oxides etc.[11–13] Graphene along with its two dimensional analogues and other heterostructures (due to their hybridisation) have been studied intensively for their possible application as electrode materials for supercapacitors.[14–17]

Many three dimensional materials are composed of numerous such two dimensional structures,[18–20] which are chemically or physically aggregated in order to form a stable morphology. In this report we have demonstrated a facile route for the synthesis of a ternary metal oxide (spinel oxide) having a micro-spherical structure. The as obtained spherical spinel oxide is formed due to the growth and aggregation of a number of two dimensional nanosheets. Spinel oxides are a new class of materials, currently drawing huge attention due to their unique, complex structure and properties as well as broader applicability.[21–24]The spinel oxide reported here is $ZnCo_2O_4$ (ZCO) which belongs to the group of normal spinels having a space symmetry group $\boldsymbol{Fd\bar{3}m} \equiv \boldsymbol{O_h^7}$.[25] Detailed electrochemical studies were performed in order to investigate the potential application of ZCO as supercapacitor electrodes.

Supercapacitors store energy in terms of both electrostatic double layer capacitance (EDLC) and pseudocapacitance. Pseudocapacitance property of a material is characterised by reversible faradic reaction caused by rapid redox activities inside a electrochemical cell. They have much faster charging capability as compared to batteries and slower discharge rate as compared to a normal capacitor. In contrast to rechargeable batteries, it can deliver an enormous amount of power required for electric vehicles and other high power consuming devices with having the additional advantage of long cyclic stability. Recently, various metal oxides such as Co_3O_4,[26] MnO_2,[27] RuO_2,[28] along with many ternary metal oxides such as $MnCo_2O_4$,[29] $NiCo_2O_4$,[4,30] and $CoMo_2O_4$[31] have shown interesting supercapacitive properties. The ZCO sample reported here is a ternary transition metal oxide synthesised by a facile hydrothermal method. The Zn and Co precursors along with urea were dissolved in de-ionised water. The dissolved urea decomposes to form CO_2 and NH_3. Further reaction of NH_3 with water (H_2O) forms NH_4OH and subsequently increases the pH of mixture solution. Under such hydrothermal condition, super-saturation occurs among the co-precipitated particles, which favors the formation of nanosheet like structures.[32–34] Further, self-assembly of those nanosheets forms thermally stable tiny spherical structures.

2. Experimental methods

All the chemicals were used as received without any alteration.

2.1. Synthesis of $ZnCo_2O_4$

[a] School of Basic Sciences, Indian Institute of Technology, Bhubaneswar, 751013, Odisha, India.
E-mail: csrout@iitbbs.ac.in

† Footnotes relating to the title and/or authors should appear here.
Electronic Supplementary Information (ESI) available: FESEM images of the sample at different time steps and cyclic voltammetry data at lower scan rates. See DOI: 10.1039/x0xx00000x

3 mmol of $Zn(NO_3)_2.6H_2O$ and 6 mmol of $Co(NO_3)_2.6H_2O$ were first dissolved in 20 ml de-ionised (DI) water and kept under constant stirring condition. An aqueous solution of urea (60 mmol of urea dissolved in 20 ml DI water) was then slowly added to the above solution and the mixture solution was further kept under constant stirring condition for 2 hrs. The as prepared final solution (40 ml) was then transferred to a 50 ml Teflon lined stainless steel autoclave and kept at 200°C for ~12 hrs. The resultant colloidal mixture was then collected via filtration and washed with DI water and absolute ethanol several times to remove any spurious content and unreacted ions. The final precipitate was then dried by keeping it inside a vacuum oven at 70 °C overnight.

2.2. Characterisation

The as-prepared sample was characterised by powder X-ray diffraction technique (Bruker D8 Advanced diffractometer having Cu-K_α radiation, λ=0.154184 nm). Morphology and elemental composition of the sample were analysed by FESEM (Merlin compact with Gemini-I electron column, Zeiss Pvt. Ltd., Germany), EDAX and elemental mapping (INCA, Oxford Instruments, UK). Raman spectrum was collected by Renishaw inVia, micro Raman spectrometer with excitation source of 532 nm.

2.3. Electrochemical measurements

The electrochemical activities of the sample were studied by taking a glassy carbon electrode (GCE) modified with the sample as the working electrode, Ag/AgCl as reference electrode and a Pt wire as the counter electrode. In a typical procedure, a glassy carbon electrode was polished thoroughly using micro-polishing powder (Al_2O_3, 0.05μm) to get a mirror finish. Then it was ultrasonicated in dilute HNO_3 to remove any kind of surface adsorbents. 1 mg of the ZCO was added to a 100 µl mixture of ethanol (95 µl) and nafion (5 µl) and was sonicated to get an ink like dispersion. 2 µl of the above dispersion was drop-casted onto the finely polished surface of the glassy carbon electrode and was vacuum dried (for about 1 hr). The modified GCE was then taken as working electrode. Cyclic Voltammetry and charge-discharge measurements were carried out in 2M aqueous KOH solution using a standard Potentiostat/Galvanostat (PG262A, Technoscience Instruments, Bangalore, India).

3. Results and discussion

A schematic representation of the formation of ZCO spherical structures is shown in Scheme 1. A time varied synthesis of ZCO was also carried out to show the progressive stages of formation of ZCO. Corresponding field emission scanning electron microscopy (FESEM) images have been provided in the supplementary data (Fig. S1). Detailed morphology of finally obtained ZCO sample was examined by FESEM along with energy dispersive X-ray spectroscopy (EDS). The FESEM images (Fig. 1a-b) elucidate entanglement of large and thin edged ZCO nanosheets. The EDS spectrum shows the composition of the sample and their atomic and weight percentages. The mapping data are shown in Fig. 2 which confirms the homogeneous distribution of the constituents of ZCO, throughout the mapping region. Fig. 3a shows the powder X-ray diffraction (XRD) patterns of ZCO nanosheets at different temperatures (i.e. 90°C, 120°C, 180°C and 200°C). It can be clearly observed that the sample synthesised at 200°C has the best crystalline and clear phase growth, though samples at 120°C and 180°C are more or less close to it. The XRD pattern obtained in case of the sample synthesised at 200°C confirmed the formation of pure phase ZCO (JCPDS file No. 23-1390) which belongs to a cubic spinel group having space symmetry $\boldsymbol{Fd\bar{3}m \equiv O_h^7}$. Raman spectra for the sample (Fig. 3b) reveals five characteristic peaks, including a shoulder/satellite peak at 658 cm^{-1} which results from $\boldsymbol{A_{1g}}$ symmetry mode. Similar vibrational mode was also observed at 682 cm^{-1} which corresponds to $\boldsymbol{A_{1g}}$ mode. Peaks appearing at 472 cm^{-1} and 512 cm^{-1} are due to the strong vibration modes $\boldsymbol{E_g}$ and $\boldsymbol{F_{2g}^{(2)}}$, respectively. The peak at 603 cm^{-1} is due to the stretching of Co-O bond and belongs to $\boldsymbol{F_{2g}^{(1)}}$ symmetry mode. All these Raman peaks can be assigned to the reported cubic spinel, ZCO.[25]

The electrochemical studies were performed by both cyclic voltammetry and charge-discharge measurements in 2M aqueous KOH solution with the help of a three electrode configuration. From the cyclic voltammetry (CV) curves, the capacitance was calculated implementing the following formula (for three electrode configuration);[35]

$$\boldsymbol{C_{sp}^{cv} = \frac{\oint I(V)dV}{mr2(V_f - V_i)} = \frac{\int_{-0.1}^{0.4} I(V)dV + \int_{0.4}^{-0.1} I(V)dV}{mr2(V_f - V_i)}} \quad (1)$$

Similarly, from the constant current charge-discharge (CCCD) measurements, the specific capacitance of the material was evaluated using the following formula;

$$\boldsymbol{C_{sp}^{cccd} = \frac{I}{ms}} \quad (2)$$

where $\boldsymbol{C_{sp}^{cv}}$ and $\boldsymbol{C_{sp}^{cccd}}$ are specific capacitances from cyclic voltammetry and constant current charge-discharge measurements respectively, $\boldsymbol{I(V)dV}$ is the area under the cyclic voltammetry curve, $\boldsymbol{m}$ is the mass of the sample drop-cast on the GCE surface, $\boldsymbol{r}$ is the scan rate, $\boldsymbol{s}$ is the slope of the discharge curve and $\boldsymbol{V_f - V_i}$ is the working potential window. Similarly, energy density ($\boldsymbol{E_d}$) and power density ($\boldsymbol{P_d}$) were calculated using the following equations (Equations 3 and 4);

$$\boldsymbol{E_d = \frac{1}{2} C_{sp}^{cv} (V_f - V_i)^2} \quad (3)$$

$$\boldsymbol{P_d = \frac{1}{2} C_{sp}^{cv} (V_f - V_i) r} \quad (4)$$

Throughout the measurement process, the potential window ($\boldsymbol{V_f - V_i}$) was kept at a value of 0.5 V (from -0.1 V to 0.4 V). Values of specific capacitance at different scan rates and current densities, and cyclic stability of the sample were calculated using the data plots obtained from the electrochemical measurements. Ragone plot was plotted to observe the overall energy density and power density of the sample. Fig. 4 shows cyclic voltammetry at different scan rates (Fig. 4a) and charge-discharge at different current densities (Fig. 4b). Obtained cyclic voltammetry curves were not of rectangular/quasi-rectangular shape which reveals the pseudocapacitive property of the ZCO sample. However, the cyclic voltammetry curves do not show prominent/sharp redox peaks though mild, broad redox couples are slightly visible at lower scan rates (i.e. 1 mV/s and 2 mV/s, see Fig. S2 in the supporting information). This property is not unique in case of supercapacitor electrodes based on metal oxides. Unlike pure faradic materials such as metal hydrides/hydroxides, metal oxides are rather called as pseudocapacitive and possess altogether different electrochemical properties (approaches the EDLC domain with the additional faradic reactions, which might or not be visually inspected).[36] The pseudocapacitive property is also significantly affected by the size of the electrode material and the process of

supercapacitor device fabrication.[37,38] In another report, Simon and Gogotsi have demonstrated that even if prominent redox peaks may not be visualised in case of metal oxides having cations with wide range of oxidation states, still they undergo a series of continuous oxidation and reduction reactions,[39] eventually producing unprecedented smooth cyclic voltammetry curves. Incidentally, the subdued oxidation and reduction peaks in case of ZCO sample reported here, overlap, which shows that it has good coulombic efficiency. Furthermore, it can clearly be observed that at higher scan rates, any such redox peaks are absent. The prime reason behind it can be attributed to the kinetically slow surface reactions at higher scan rates. And the major contribution is from the double layer effect arising due to the adsorption of OH^- ions by ZCO.[40] As the faradic reaction is on the slower side at higher sweep rates, therefore the capacitance decreases gradually. That is why the sample showed a specific capacitance of 1654 F/g at a sweep rate of 1 mV/s, whereas at a scan rate of 200 mV/s, the value obtained was 694 F/g. The charge-discharge curves are nearly triangular and highly symmetric in shape which suggests that the sample has very high coulombic efficiency and the faradic reactions taking place are highly reversible in nature. Also the immediate discharge without any significant amount of IR drop suggests low internal resistance of the sample. Fig. 4c and Fig. 4d depict the variations of specific capacitance with scan rate and current density, respectively. The capacitance shown by the sample is by virtue of two different contributions, one is from fast redox reaction and the other is from EDLC. These two contributions were calculated separately using the discharge curves by following a method detailed in a previous report.[41] At a current density of 1 A/g, the ratio of EDLC to pseudocapacitance was found to be ($\frac{317}{488} = \sim \mathbf{0.65}$), while for a current density of 20 A/g, the ratio obtained was $\frac{5.2}{3.2} = \sim \mathbf{1.625}$, which clearly shows that at lower current densities, contribution from pseudocapacitance is much larger than that of EDLC, whereas for higher current densities, EDLC plays major role towards electrochemical supercapacitor performance of the sample. A long cyclic stability test, in terms of 5000 charge-discharge cycles (at a current density of 20 A/g) has been performed for the ZCO sample which is shown in Fig. 5. The cycle number versus capacity retention plot is illustrated in Fig. 5a. The first 5 cycles and last 5 cycles are provided in Fig. 5b and 5c, respectively which shows little distortion in the shape of the charge-discharge curves even after 5000 cycles. It was found that the retention power of the ZCO sample decreased to ~78% of its initial value. Morphology of the sample was investigated after 5000 charge-discharge cycles with the help of field emission scanning electron microscopy (see Fig. S3 in the supporting information). Supercapacitor performance of the ZCO sample, in terms of energy density and power density has been elucidated in Fig. 5c, through a Ragone plot.

The ZCO sample reported here possess promising electrochemical supercapacitive performances and comparable to recently reported data on ZCO having different structures, and fabrication procedures. Nanorod structured ZCO grown on nickel foam has been reported to have a specific capacitance of ~1400 F/g at a current density of 1 A/g.[42] A specific capacitance of 647 F/g at a current density of 1 A/g has been also been reported for porous ZCO microspherical structures.[43] The as reported ZCO sample has micro-spherical shape consisting of numerous nanosheets which have thickness in the nanometer range, and possess highly rough surfaces with imperfect growth at edges, enabling the possibility of better ion-trapping capabilities. The three dimensional structure has also got numerous prominent pores which provides an active path for the diffusion of electrolyte, facilitating much improved ion/electron transportation. The morphological peculiarity is further corroborated by the detailed electrochemical investigations in a three-electrode configuration taking 2M aqueous KOH solution as the electrolyte. The sample showed enhanced supercapacitor properties as compared to the previous reports and thus has enough potential for its application as an active material for the fabrication of high performance supercapacitor devices. A detailed comparison of the supercapacitor performances of various reported metal oxides have been provided in Table 1.

Table 1. Comparison of supercapacitor performance of various metal oxides and their composite structures.

Electrode Material	Highest Specific Capacita-nce	Capacity Retention (<1000 cycles)	Max. Energy Density (Wh/Kg)	Max. Power Density (KW/Kg)	Reference
Self-assembled $ZnCo_2O_4$ nanosheets	1550 F/g (at 1 A/g)	~78%	57.4	34.7	Present work
$ZnCo_2O_4$ porous nanotube	770 F/g (at 10 A/g)	~94.1%	25	15.3	44
$ZnCo_2O_4$ micro-spheres	953.2 F/g (at 4 A/g)	97.8%	33.1	8	45
$MnCo_2O_4$ nanostructure	346 F/g (1 A/g)	~88%	-----	-----	46
3D-nanonet Co_3O_4	739 F/g (at 1 A/g)	~90.2%	16.42	3	47
$NiMoO_4$ microsphere	974.4 F/g (1 A/g)	~74.5%	32.2	2.1	48
3D $NiCo_2O_4$ microsphere	1284 F/g (2 A/g)	~97.5%	-----	-----	30
NiO nanocompo-site	429.7 F/g (0.2 A/g)	~86.1%	-----	-----	49

4. Conclusions

In summary, a facile synthesis method for ZCO nanosheets has been reported here and their supercapacitor performance was tested thoroughly in an alkaline medium (2M KOH) which showed an energy density of 57.4 Wh/Kg and high specific capacitance of 1654 F/g. All the analyses show that these ZCO nanosheet structures have promising applicability as low-cost, environmentally friendly and high performance supercapacitor electrodes.

Acknowledgements

Dr. C.S. Rout would like to thank DST (Government of India) for the Ramanujan fellowship (Grant No. SR/S2/RJN-21/2012). This work was supported by the DST-SERB Fast-track Young scientist (Grant No. SB/FTP/PS-065/2013), UGC-UKIERI thematic awards (Grant No.

UGC-2013-14/005) and BRNS-DAE, (Grant No. 37(3)/14/48/2014-BRNS/1502). Also, part of this work is supported by the Indo-US Science and Technology Forum (IUSSTF) through a joint INDO-US centre grant and Ministry of Human Resources Development (MHRD), India through a center of excellence grant.

Notes and references

1 H. Sun, J. Deng, L. Qiu, X. Fang and H. Peng, *Energy Environ. Sci.*, 2015, **8**, 1139–1159.

2 H. Huang and X. Wang, *J. Mater. Chem. A*, 2014, **2**, 6266–6291.

3 S. Goriparti, E. Miele, F. De Angelis, E. Di Fabrizio, R. Proietti Zaccaria and C. Capiglia, *J. Power Sources*, 2014, **257**, 421–443.

4 T.-Y. Wei, C.-H. Chen, H.-C. Chien, S.-Y. Lu and C.-C. Hu, *Adv. Mater.*, 2010, **22**, 347–351.

5 Y. Sun, Q. Wu and G. Shi, *Energy Environ. Sci.*, 2011, **4**, 1113–1132.

6 F. Bonaccorso, L. Colombo, G. Yu, M. Stoller, V. Tozzini, A. C. Ferrari, R. S. Ruoff and V. Pellegrini, *Sci.*, 2015, **347**, 1246501.

7 A. H. Castro Neto, N. M. R. Peres, K. S. Novoselov and A. K. Geim, *Rev. Mod. Phys.*, 2009, 81, 109–162.

8 A. K. Geim, *Sci.* , 2009, **324** , 1530–1534.

9 A. K. Geim and K. S. Novoselov, *Nat. Mater.*, 2007, **6**, 183–191.

10 G. A. Muller, J. B. Cook, H.-S. Kim, S. H. Tolbert and B. Dunn, *Nano Lett.*, 2015, **15**, 1911–1917.

11 Z. Sun, T. Liao, Y. Dou, S. M. Hwang, M.-S. Park, L. Jiang, J. H. Kim and S. X. Dou, *Nat Commun*, 2014, **5**, 3813.

12 E. Kan, M. Li, S. Hu, C. Xiao, H. Xiang and K. Deng, *J. Phys. Chem. Lett.*, 2013, **4**, 1120–1125.

13 M. Pandey, A. Vojvodic, K. S. Thygesen and K. W. Jacobsen, *J. Phys. Chem. Lett.*, 2015, **6**, 1577–1585.

14 H. Wang, H. Feng and J. Li, *Small*, 2014, **10**, 2165–2181.

15 J. J. Yoo, K. Balakrishnan, J. Huang, V. Meunier, B. G. Sumpter, A. Srivastava, M. Conway, A. L. Mohana Reddy, J. Yu, R. Vajtai and P. M. Ajayan, *Nano Lett.*, 2011, **11**, 1423–1427.

16 S. Peng, L. Li, H. Tan, R. Cai, W. Shi, C. Li, S. G. Mhaisalkar, M. Srinivasan, S. Ramakrishna and Q. Yan, *Adv. Funct. Mater.*, 2014, **24**, 2155–2162.

17 S. Ratha and C. S. Rout, *ACS Appl. Mater. Interfaces*, 2013, **5**, 11427–11433.

18 B. Huang, M. Cao, B. Cheng, J. Sun, N. Li, F. Nie, H. Zhang, H. Huang and C. Hu, *Cryst. Growth Des.*, 2012, **12**, 3418–3425.

19 J. Guo, J. Zhang, D. Ju, H. Xu and B. Cao, *Powder Technol.*, 2013, **250**, 40–45.

20 J. Li, G. Lu, Y. Wang, Y. Guo and Y. Guo, *J. Colloid Interface Sci.*, 2012, **377**, 191–196.

21 J. Y. C. Chen, J. T. Miller, J. B. Gerken and S. S. Stahl, *Energy Environ. Sci.*, 2014, **7**, 1382–1386.

22 V. Kocsis, S. Bordács, D. Varjas, K. Penc, A. Abouelsayed, C. A. Kuntscher, K. Ohgushi, Y. Tokura and I. Kézsmárki, *Phys. Rev. B*, 2013, **87**, 64416.

23 J. Zhang, X.-G. Zhang and X. F. Han, *Appl. Phys. Lett.*, 2012, **100**, 222401.

24 Y. Liang, H. Wang, J. Zhou, Y. Li, J. Wang, T. Regier and H. Dai, *J. Am. Chem. Soc.*, 2012, **134**, 3517–3523.

25 S. Ratha, R. T. Khare, M. A. More, R. Thapa, D. J. Late and C. S. Rout, *RSC Adv.*, 2014, **5**, 5372–5378.

26 C. Feng, J. Zhang, Y. He, C. Zhong, W. Hu, L. Liu and Y. Deng, *ACS Nano*, 2015, **9**, 1730–1739.

27 J. Kang, A. Hirata, L. Kang, X. Zhang, Y. Hou, L. Chen, C. Li, T. Fujita, K. Akagi and M. Chen, *Angew. Chemie*, 2013, **125**, 1708–1711.

28 N. Yoshida, Y. Yamada, S. Nishimura, Y. Oba, M. Ohnuma and A. Yamada, *J. Phys. Chem. C*, 2013, **117**, 12003–12009.

29 L.-B. Kong, C. Lu, M.-C. Liu, Y.-C. Luo, L. Kang, X. Li and F. C. Walsh, *Electrochim. Acta*, 2014, **115**, 22–27.

30 R. Zou, K. Xu, T. Wang, G. He, Q. Liu, X. Liu, Z. Zhang and J. Hu, *J. Mater. Chem. A*, 2013, **1**, 8560–8566.

31 D. Guo, H. Zhang, X. Yu, M. Zhang, P. Zhang, Q. Li and T. Wang, *J. Mater. Chem. A*, 2013, **1**, 7247–7254.

32 M. L. Kieke, J. W. Schoppelrei and T. B. Brill, *J. Phys. Chem.*, 1996, **100**, 7455–7462.

33 M. Oikawa and S. Fujihara, *J. Solid State Chem.*, 2005, **178**, 2036–2041.

34 K. Kakiuchi, E. Hosono, T. Kimura, H. Imai and S. Fujihara, *J. Sol-Gel Sci. Technol.*, 2006, **39**, 63–72.

35 S. Ratha, S. R. Marri, N. a. Lanzillo, S. Moshkalev, S. K. Nayak, J. N. Behera and C. S. Rout, *J. Mater. Chem. A*, 2015, **3**, 18874–18881.

36 T. Brousse, D. Bélanger and J. W. Long, *J. Electrochem. Soc.* , 2015, **162** , A5185–A5189.

37 V. Augustyn, P. Simon and B. Dunn, *Energy Environ. Sci.*, 2014, **7**, 1597–1614.

38 P. Simon, Y. Gogotsi and B. Dunn, *Sci.* , 2014, **343** , 1210–1211.

39 P. Simon and Y. Gogotsi, *Nat. Mater.*, 2008, **7**, 845–854.

40 H. Wu, Z. Lou, H. Yang and G. Shen, *Nanoscale*, 2015, **7**, 1921–1926.

41 Z. Lu, Z. Chang, W. Zhu and X. Sun, *Chem. Commun.*, 2011, **47**, 9651–9653.

42 B. Liu, B. Liu, Q. Wang, X. Wang, Q. Xiang, D. Chen and G. Shen, *ACS Appl. Mater. Interfaces*, 2013, **5**, 10011–10017.

43 Q. Wang, L. Zhu, L. Sun, Y. Liu and L. Jiao, *J. Mater. Chem. A*, 2015, **3**, 982–985.

44 G. Zhou, J. Zhu, Y. Chen, L. Mei, X. Duan, G. Zhang, L. Chen, T. Wang and B. Lu, *Electrochim. Acta*, 2014, **123**, 450–455.

45 Q. Wang, J. Du, Y. Zhu, J. Yang, J. Chen, C. Wang, L. Li and L. Jiao, *J. Power Sources*, 2015, **284**, 138–145.

46 N. Padmanathan and S. Selladurai, *Ionics (Kiel).*, 2014, **20**, 479–487.

47 Y. Wang, Y. Lei, J. Li, L. Gu, H. Yuan and D. Xiao, *ACS Appl. Mater. Interfaces*, 2014, **6**, 6739–6747.

48 D. Cai, D. Wang, B. Liu, Y. Wang, Y. Liu, L. Wang, H. Li, H. Huang, Q. Li and T. Wang, *ACS Appl. Mater. Interfaces*, 2013, **5**, 12905–12910.

49 Y. Jiang, D. Chen, J. Song, Z. Jiao, Q. Ma, H. Zhang, L. Cheng, B. Zhao and Y. Chu, *Electrochim. Acta*, 2013, **91**, 173–178.

Figure Captions:

Scheme 1 Illustration of the mechanism behind the formation of ZCO spherical structures.

Fig. 1 FESEM images of ZCO sample at (a) low magnification and (b) high magnification. (c) EDS with atomic and weight percentage composition of the sample.

Fig. 2 Elemental mapping data for ZCO sample. (a) electron image over which the mapping has been done. Presence of (a) oxygen, (b) zinc and (c) cobalt is confirmed.

Fig. 3 (a) X-ray diffraction pattern for ZCO at different temperatures and (b) Raman spectroscopy data.

Fig. 4 Electrochemical measurement data for ZCO. (a) cyclic voltammetry curves at different scan rates, (b) charge-discharge curves at different current densities and the variation of specific capacitance with respect to (c) scan rate and (d) current density.

Fig. 5 (a) Capacity retention power of the ZCO sample in percentage calculated from 5000 charge-discharge cycles. (b) Initial and (c) last 5 charge-discharge curves taken from the 5000 cycle data. (c) Ragone plot, establishing a relation between energy density and power density.

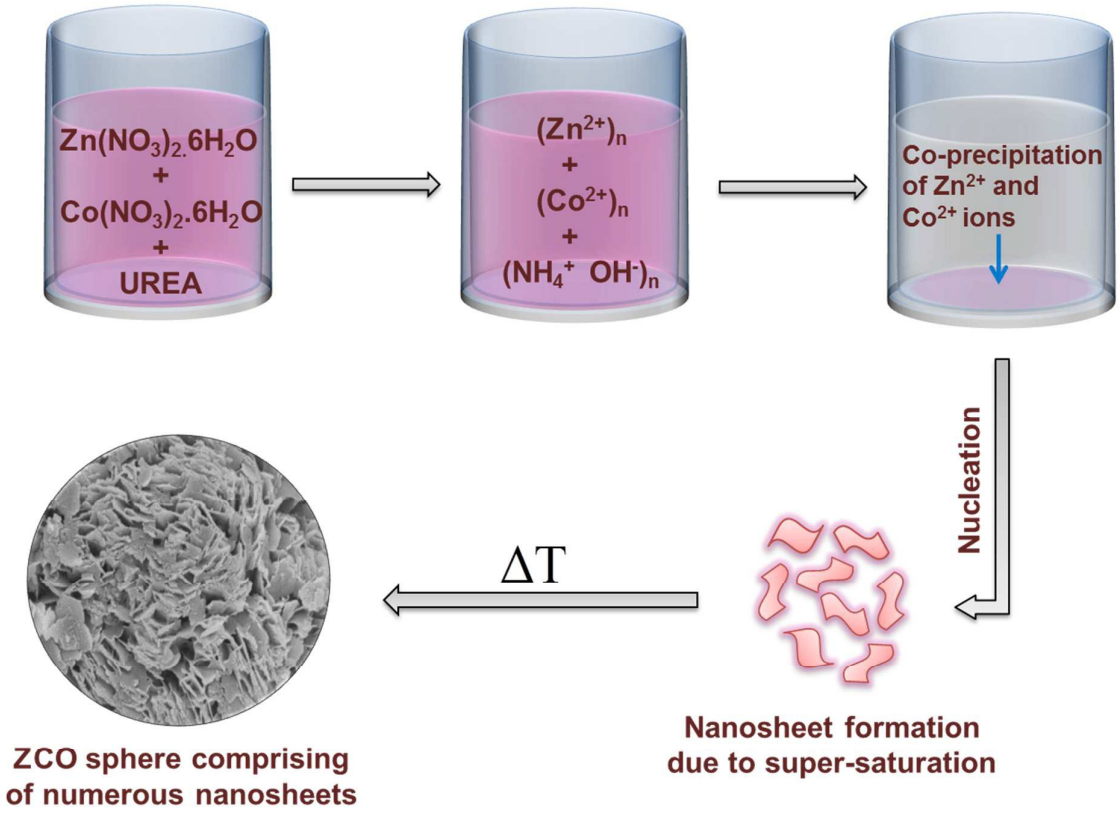

Scheme 1

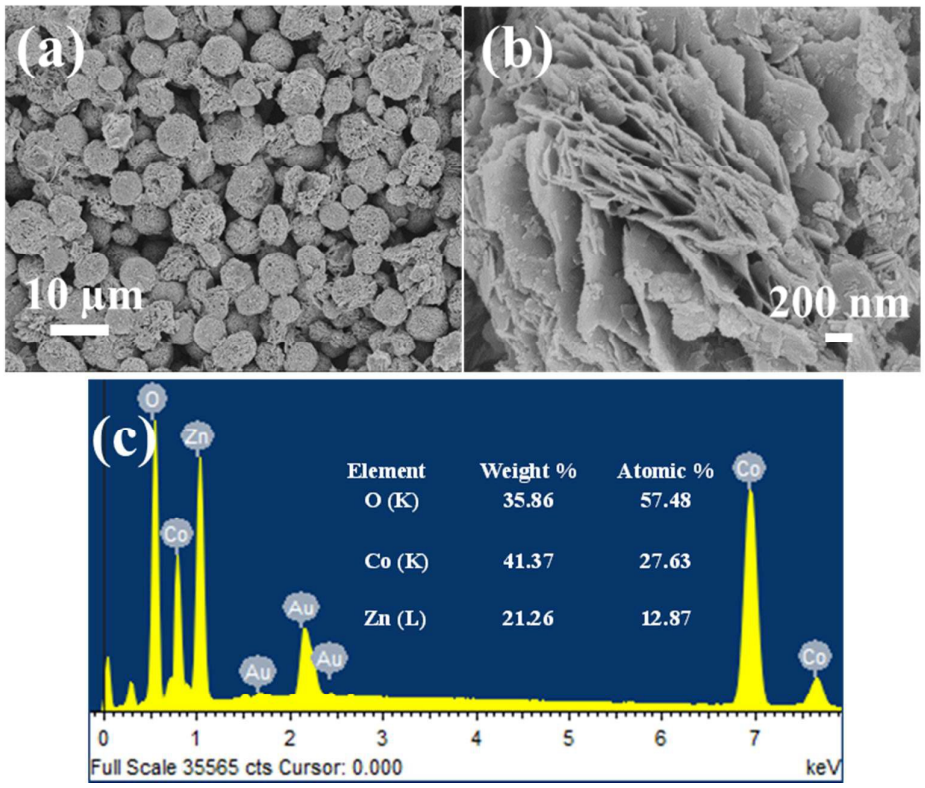

Figure 1

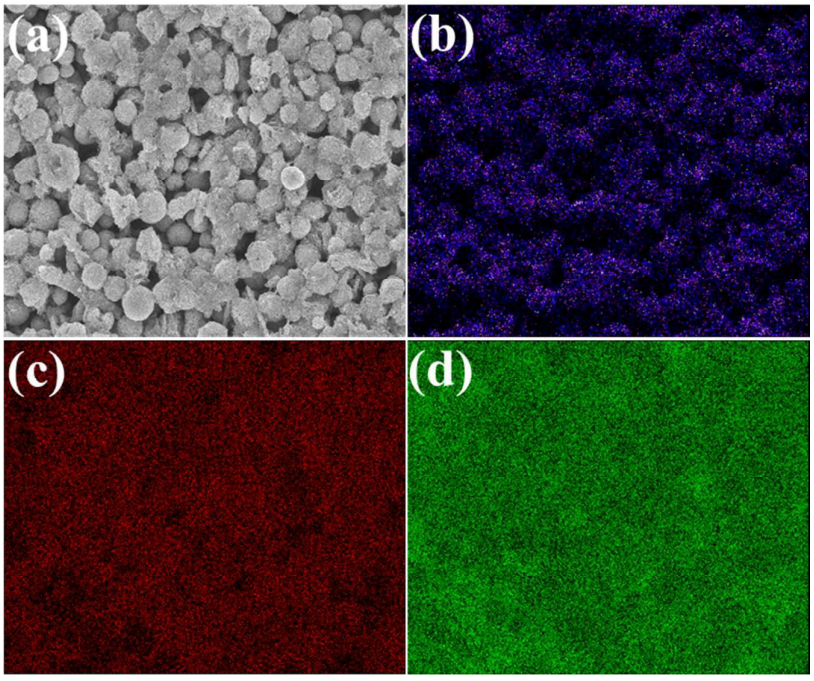

Figure 2

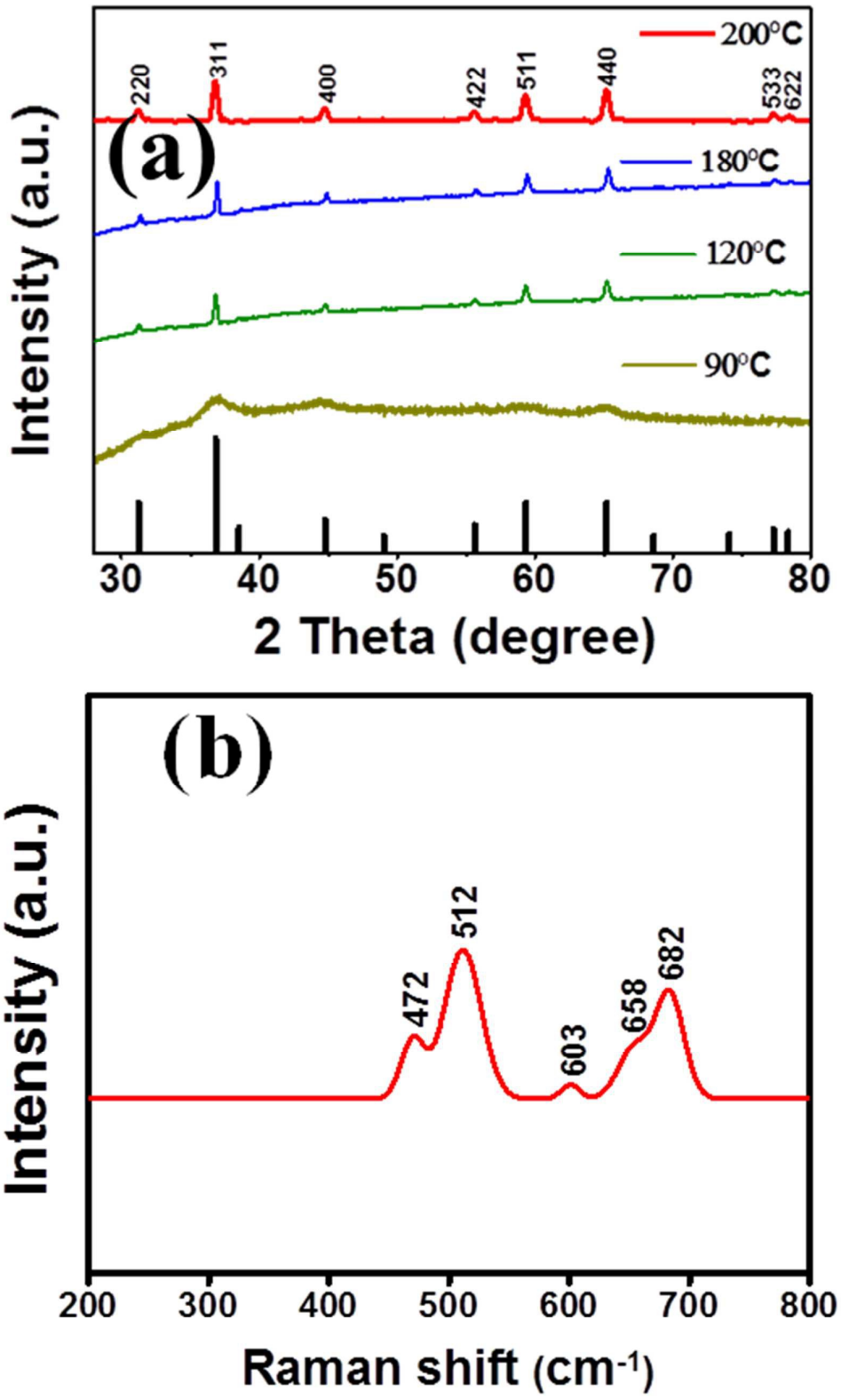

Figure 3

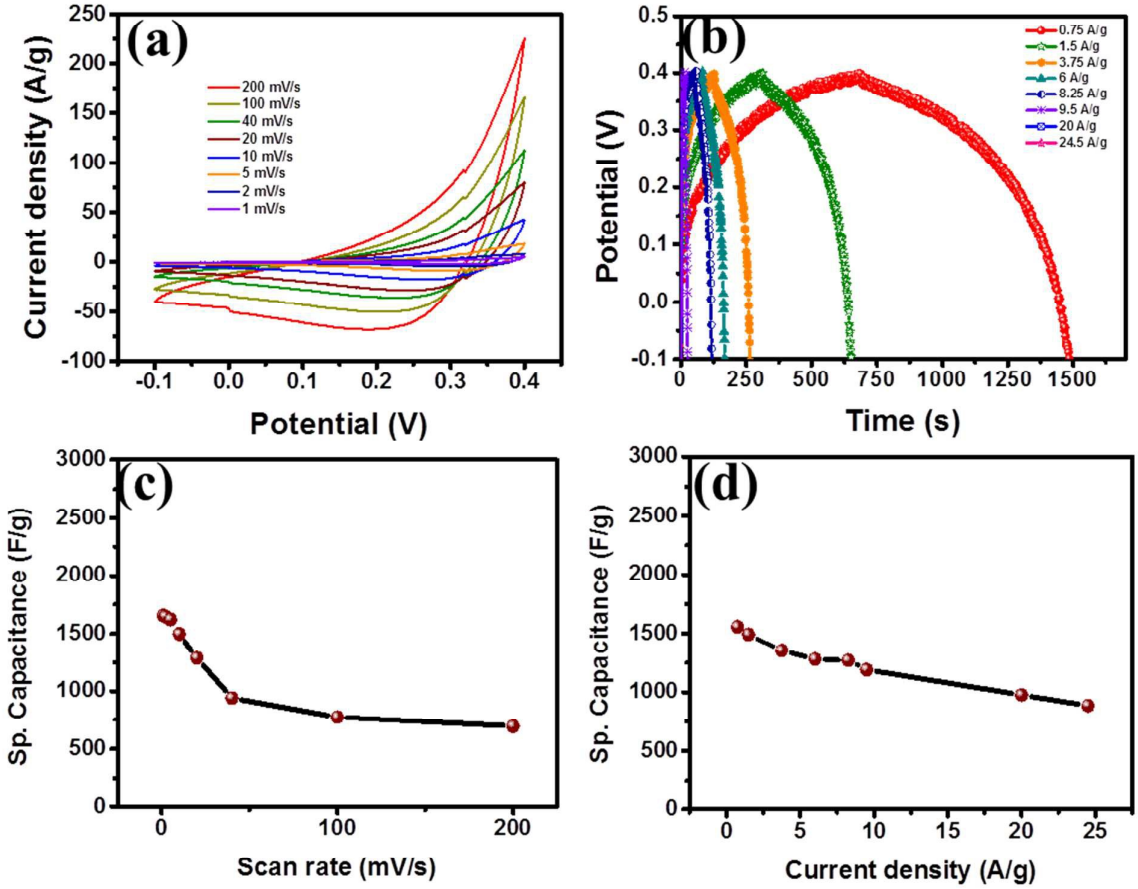

Figure 4

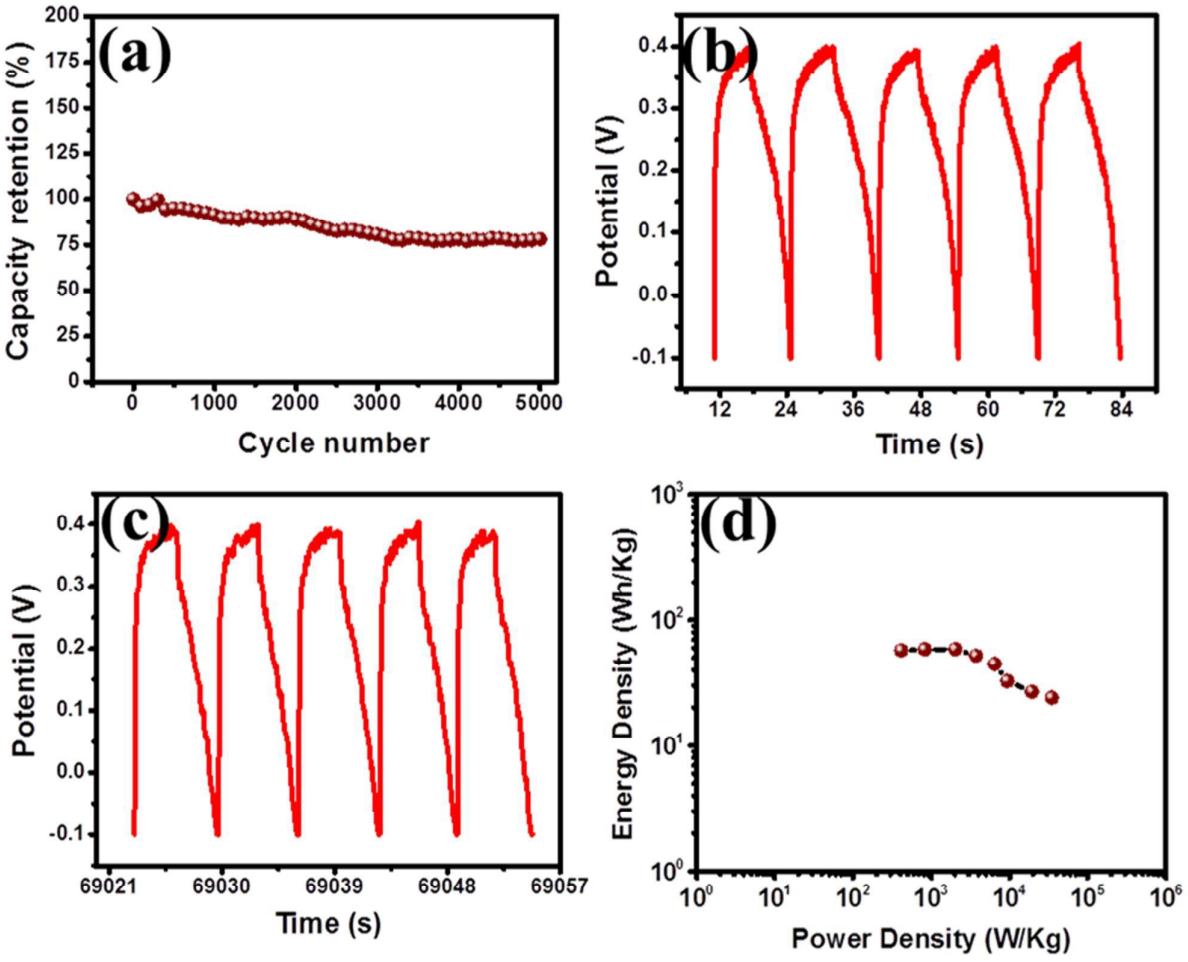

Figure 5

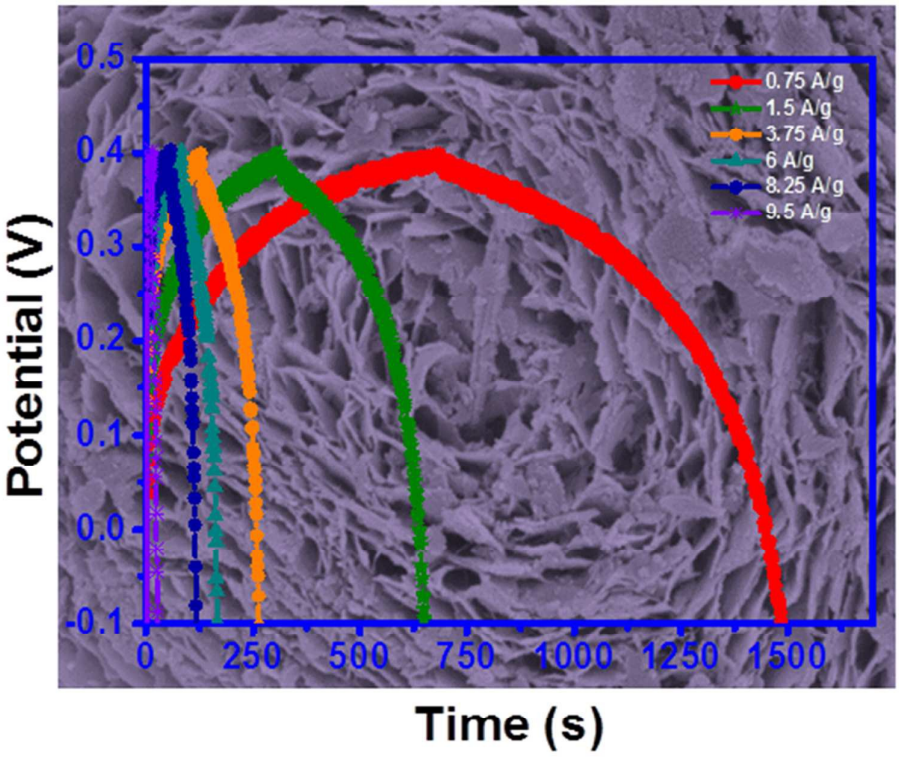

TOC Figure